Journal of Materials Chemistry C

Photoluminescence property of quinary Ag-(In,Ga)-(S,Se) quantum dots with a gradient alloy structure for in vivo bioimaging

Journal:	*Journal of Materials Chemistry C*
Manuscript ID	TC-ART-06-2021-002746.R1
Article Type:	Paper
Date Submitted by the Author:	26-Jul-2021
Complete List of Authors:	Rismaningsih, Nurmanita; Nagoya University, Materials Chemistry Yamauchi, Hiroki; Nagoya University, Graduate School of Engineering Kameyama, Tatsuya; Nagoya University, Graduate School of Engineering Yamamoto, Takahisa; Nagoya University, Graduate School of Engineering Morita, Saho; Nagoya University, Materials Chemistry Yukawa, Hiroshi; Nagoya Daigaku Kogakubu Daigakuin Kogaku Kenkyuka, Uematsu, Taro; Osaka University, Department of Applied Chemistry, Graduate School of Engineering Baba, Yoshinobu; Nagoya University, ImPACT Research Center for Advanced Nanobiodevices Kuwabata, Susumu; Osaka University, Department of Applied Chemistry, Graduate School of Engineering Torimoto, Tsukasa; Nagoya University, Graduate School of Engineering

ARTICLE

Photoluminescence property of quinary Ag-(In,Ga)-(S,Se) quantum dots with a gradient alloy structure for *in vivo* bioimaging

Received 00th January 20xx,
Accepted 00th January 20xx

DOI: 10.1039/x0xx00000x

Nurmanita Rismaningsih,[a] Hiroki Yamauchi,[a] Tatsuya Kameyama,[a] Takahisa Yamamoto,[a] Saho Morita,[a] Hiroshi Yukawa,[a,b,c] Taro Uematsu,[d] Yoshinobu Baba,[a,b,c] Susumu Kuwabata[d] and Tsukasa Torimoto*[a,b]

Multinary semiconductor quantum dots (QDs) composed of group I-III-VI elements have received much attention for wide-ranging applications due to their low level of toxicity and tunable optical properties. The chemical composition and particle size are important parameters for controlling the physicochemical properties of these QDs. In this study, we prepared quinary QDs of an Ag-(In,Ga)-(S,Se) semiconductor (AIGSSe) by thermolysis of precursors in an organic solution with two-step heat treatment and evaluated their physicochemical properties as a function of the Se fraction. The energy gap (E_g) of QDs decreased from 1.9 to 1.5 eV with an increase in the Se/(S+Se) ratio from 0 to 1, accompanied by a shift of the valence band maximum to a higher energy level. The obtained AIGSSe QDs exhibited a sharp band-edge PL peak, the wavelength of which was red-shifted from 580 to 790 nm with a decrease in their E_g. The PL intensity was remarkably enlarged by the surface coating with a GaS_x shell, the highest PL quantum yield being 50% for the PL peak at 580 nm. AIGSSe QDs with an Se/(S+Se) ratio of 0.50 exhibited a near-IR PL peak at 790 nm, which is suitable for *in vivo* bioimaging in the wavelength range of the first biological window. By incorporating GaS_x-coated AIGSSe QDs (Se/(S+Se)= 0.50) into liposomes, the QDs were transferred into aqueous solutions without significant deterioration of both the PL peak outline and quantum yield, though a broad PL peak originating from defect sites appeared with a relatively large PL intensity when GaS_x-coated Ag-(In,Ga)-S QDs that did not contain Se were used. *In vivo* imaging of a mouse was successfully performed by detecting the band-edge emission at 790 nm of AIGSSe QDs injected subcutaneously in the back of the mouse.

Introduction

Optical imaging of biological tissues and cells is generally carried out under ambient temperature and pressure conditions and it has been a promising technique for assessment of biological and biochemical processes. Since light in the near-IR wavelength region of the first biological window (700~900 nm) and the second biological window (1000~1400 nm) can penetrate deeply into biological tissues with reduced autofluorescence[1-3], binary quantum dots (QDs) exhibiting near-IR photoluminescence (PL), such as CdSe[4,5], CdTe[6,7], and PbS[8,9], have been intensively investigated as materials to replace organic dyes or fluorescent proteins, which have relatively low brightness and less tolerance for photobleaching.[10-13] These binary QDs with relatively narrow energy gaps (E_gs) have been prepared by well-established solution-phase methods and exhibited narrow band-edge PL peaks in the visible and near-IR regions, the wavelength of which was strongly dependent on the particle size. However, notable toxicity and a potential environmental hazard associated with the contents of Cd or Pb atoms have greatly limited the practical use of these QDs.[14]

On the other hand, multinary I-III-VI-based semiconductors such as $AgInS_2$,[15-22] $AgInSe_2$,[23-25] $CuInS_2$,[26-34] and $CuInSe_2$[35-37] have attracted much attention for practical applications in diverse fields from light-emitting diodes, bioimaging, and solar cells to photocatalytic applications. The advantages of these materials include direct band gap semiconductors with strong absorption coefficients from visible to near-IR wavelength regions as well as less-toxic composition. Quantum dots consisting of multinary elements also have flexible properties that can be controlled by adjusting both their particle size and chemical composition.[38] Since I-III-VI semiconductors can make alloys with II-VI semiconductors or different I-III-VI semiconductors, QDs composed of mixed-cation alloys have been intensively investigated. For example, multinary QDs composed of alloys of ZnS and $AgInS_2$ or alloys of ZnS and $CuInS_2$ have been reported to have tunable E_gs depending on the fraction of Zn in QDs and they showed broad photoluminescence (PL) peaks in a wide visible wavelength region, the wavelength of the PL peak being controlled by

[a] Graduate School of Engineering, Nagoya University, Chikusa-ku, Nagoya 464-8603, Japan. E-mail: torimoto@chembio.nagoya-u.ac.jp
[b] Institute of Nano-Life-Systems, Institutes of Innovation for Future Society, Nagoya University, Chikusa-ku, Nagoya 464-8603, Japan.
[c] Institute for Quantum Life Science, Quantum Life and Medical Science Directorate, National Institutes for Quantum and Radiological Science and Technology, Inage-ku, Chiba 263-8555, Japan.
[d] Graduate School of Engineering, Osaka University, 2-1 Yamada-oka, Suita, Osaka 565-0871, Japan

changing the E_g of QDs with their chemical composition or their particle size.[39,40] Furthermore, Wang and co-workers developed ZnAgInSe and ZnCuInSe quantum dots that have a broad photoluminescence (PL) peak, the peak wavelength being controllable from 550 to 820 nm and from 570 to 820 nm, respectively, with cation ratios of Zn/Ag/In and Zn/Cu/In in QDs, respectively.[41] Since PL quantum yields (QYs) were improved by surface coating with a ZnS shell up to 70%, the resulting QDs were proven to be photoluminescent probes for bioimaging after modification with a water transfer agent. It was reported by Mir et al. that $AgInS_2$@ZnS exhibited a tunable band gap ranging from 2.4 to 3.5 eV for high-contrast cell imaging, in which a broad PL peak appeared in the visible wavelength region (500 to 600 nm), depending on the ratio of Ag/In in the precursors.[16] Recently we reported that off-stoichiometric Ag-In-Ga-S (AIGS) QDs, synthesized by Ga^{3+} doping into Ag-In-S QDs in solutions, exhibited a sharp band-edge PL peak as well as a broad defect-site emission, in which the peak wavelength of the band-edge peak was blue-shifted from 610 to 500 nm with an increase in the amount of Ga^{3+} doping.[42] Furthermore, coating AIGS QDs with a GaS_x shell remarkably suppressed the broad defect-site PL peak and then the optimal PL QY of ca. 28% was obtained for a green band-edge emission at 530 nm of AIGS@GaS_x core-shell QDs. By replacing S in AIGS with Se, we prepared multinary QDs showing PL in the first biological near-IR window. An off-stoichiometric Ag-In-Ga-Se (AIGSe) semiconductor predominantly exhibited a sharp band-edge emission by surface coating with a GaS_x shell, and the peak wavelength was blue-shifted from 890 to 630 nm with an increase in the Ga^{3+} fraction in the AIGSe core.[23] These AIGSe@GaS_x QDs were successfully used as near-IR PL probes for three-dimensional *in vivo* bioimaging, but their PL QY considerably decreased from 14.2% to 6.2% after transfer from chloroform to aqueous solutions.

Mixed-anion I-III-VI-based QDs have also been prepared by solution-phase methods, and their optical properties were controlled by individual fractions of anion constituents. For example, it has been reported that the E_gs of $CuIn(S,Se)_2$[43] and $AgIn(S,Se)_2$[44] QDs, synthesized by heating-up methods were tunable by changing the S/Se ratio in precursors. Yun and co-workers observed that nanoparticle films composed of $CuIn(S,Se)_2$ QDs with a broad PL peak exhibited a remarkable increase of carrier mobilities with an increase in the Se fraction in QDs.[45] Song et al. reported the QD-sensitized solar cells prepared with Zn-Cu-In-S-Se QDs showed a solar energy conversion efficiency of 14.4%, the value of which was highest among those reported for liquid-junction QD solar cells.[46] Most research works have focused on the preparation of near-IR-absorptive QDs for applications to solar light energy conversion systems.[47-50] Although mixed-anion alloy QDs are also promising materials as near-IR-PL probes, there have been few reports of the use of these QDs in bioimaging because of their weak broad PL peak originating from defect sites. To improve the performance of bioimaging with mixed-anion QDs, a sharp band-edge emission in the near-IR region is preferable, but, to the best of our knowledge, such an attempt has never been done.

Here, we report a solution-phase method for synthesis of quinary QDs consisting of Ag-(In,Ga)-(S,Se) solid solution (AIGSSe) in which the optical properties and electronic energy structure were controlled by varying the Se fraction in QDs. The QDs were incorporated into liposomes to be uniformly dispersed in an aqueous solution, in which AIGSSe QDs exhibited superior durability of band-edge photoluminescence to that of their counterpart without containing Se as a constituent. We successfully performed *in vivo* PL bioimaging in the first biological NIR window with GaS_x-coated AIGSSe QDs with a band-edge PL peak.

Experimental

Materials

Metal salts of gallium (III) acetylacetonate ($Ga(acac)_3$) and indium (III) acetylacetonate ($In(acac)_3$) were purchased from Sigma-Aldrich, and silver acetate (Ag(OAc)) was obtained from Kishida Reagents Chemicals. Chalcogen compounds of thiourea and selenourea were supplied by Kishida Reagents Chemicals and Sigma-Aldrich, respectively. Solvents used for QD synthesis were oleylamine (OLA, Sigma-Aldrich) and 1-dodecanethiol (DDT, FUJIFILM Wako Pure Chemical Corporation). Other chemicals were purchased from Kishida Reagents Chemicals. All reagents were used as received without further purification. Aqueous solutions were prepared with purified water just before use by a Millipore Milli-Q system.

Solution-phase synthesis of Ag-In-Ga-S-Se (AIGSSe) quantum dots.

AIGSSe QDs were synthesized by a heating-up method with a two-step heating process, being slightly modified from our previous one.[23] Mixed powders of 0.17 mmol Ag(OAc), 0.10 mmol $In(acac)_3$, and 0.15 mmol $Ga(acac)_3$ were used as a metal precursor. A total 0.46 mmol of thiourea and selenourea was used as a chalcogen precursor for S^{2-} and Se^{2-}. The ratio of cation charge to anion charge was fixed to 1:1. The molar ratio of Ag/(Ag+In+Ga) was constantly controlled at 0.40, and the molar ratio of In/(In+Ga) was maintained at 0.40. Both the metal precursor and chalcogen precursor were added to a test tube followed by the addition of a mixed solution of 2.75 cm^3 OLA and 0.25 cm^3 DDT. After degassing the thus-prepared suspension, two-step heating was conducted under an N_2 atmosphere with vigorous stirring. The two-step heating involved heating the suspension at 100 ^oC for 30 min immediately followed by heating at 250 ^oC for 30 min. The resulting solution was cooled to room temperature and was then subjected to centrifugation at 4000 rpm for 5 min to remove aggregated large particles. A ca. 5-cm^3 portion of methanol was added to the supernatant to precipitate target AIGSSe QDs. Thus-obtained wet QD precipitates were washed several times with methanol and ethanol and were then dissolved in chloroform (3 cm^3) for further experiments.

Surface coating of AIGSSe QDs with GaS_x shells.

We prepared core-shell-structured AIGSSe@GaS_x QDs by a previously reported method with a slight modification.[23] AIGSSe

QDs (10 nmol(QDs)) were added to 3.0 cm^3 OLA containing 53 μmol of $Ga(acac)_3$ and 53 μmol of thiourea. The resulting mixture was heated at 300 °C for 15 min with vigorous stirring under an N_2 atmosphere. The obtained solution was cooled to room temperature followed by centrifugation at 4000 rpm for 5 min to remove large particles. Target AIGSSe@GaS_x QDs were isolated from the supernatant and purified by the above-described procedure.

Characterization of quantum dots.

Absorption spectra were obtained using an Agilent 8453A diode array spectrophotometer. A photonic multichannel analyzer (Hamamatsu, PMA-12, C10027-02) was used for measurement of PL spectra, in which the wavelength of excitation light was 365 nm. The PL QY was evaluated using an absolute PL quantum yield measurement system (Hamamatsu, C9920-03) with an excitation light of wavelength at 365 nm. The crystal structures of QDs were analyzed by measuring their X-ray diffraction (XRD) patterns with an X-ray diffractometer (Rigaku, SmartLab-3K) with Cu Kα radiation. Wide-area transmission electron microscope (TEM) images were obtained with a Hitachi H-7650 TEM at an operation voltage of 100 kV and were used for analysis of the size distribution of QDs. TEM samples were prepared by dropping a QD chloroform solution onto a Cu TEM grid covered with an amorphous carbon overlayer (Okenshoji Co., Ltd., ELS-C10 STEM Cu100P grid), followed by drying. Images of high-angle annular dark-field scanning transmission electron microscopy (HAADF-STEM) were obtained with a Cs-corrected HR-STEM (JEOL Co. Ltd., ARM-200F) with an acceleration voltage of 200 kV. Nanoscale elemental analysis was also carried out with energy-dispersive X-ray spectroscopy (EDS) during the HAADF-STEM measurements. The chemical composition of QDs was analyzed by X-ray fluorescence spectroscopy (Rigaku, NEX CG) or energy dispersive X-ray spectroscopy (Horiba, Emax Energy EX-250). Photoelectron yield spectroscopy in air (PYSA) (Riken Keiki, AC-2) was used to determine the ionization energy.

AIGSSe@GaS_x application for *in vivo* imaging in mice.

The potential application of AIGSSe@GaS_x as a near-IR light-emitting probe for *in vivo* imaging was investigated using procedures similar to those previously reported.[23] The obtained AIGSSe@GaS_x QDs were surface-coated with a hydrophobic organic layer composed of OLA and then could not be uniformly dispersed in aqueous solutions. Therefore, unilamellar liposomes of 1,2-distearoyl-sn-glycero-3-phosphocholine (DSPC) were used to transfer QDs into aqueous solutions. Four nmol(QDs) of AIGSSe@GaS_x prepared with Se/(S+Se) = 0 or 0.5 was uniformly dispersed in 2 cm^3 chloroform containing 8.86 μmol of DSPC. During sonication of water (3 cm^3) for 5 min in a separate test tube, a ca. 0.5-cm^3 portion of the QDs-DSPC chloroform solution was added to the water. The obtained mixture was heated at 65 °C for 10 min to remove excess chloroform. The thus-obtained dispersion contained AIGSSe@GaS_x QDs encapsulated with DSPC liposomes (DSPC-AIGSSe@GaS_x). The average hydrodynamic diameter of the composite liposomes was determined by dynamic light scattering measurement (DLS; Otsuka Electronics FDLS-3000H).

The PL durability of DSPC-AIGSSe@GaS_x liposomes was evaluated in various conditions. After diluting original liposome dispersions to give absorbance of 0.1 at 500 nm with water, the dispersions were stored in a refrigerator at 4 °C under various conditions and then their PL spectra were measured intermittently. A monochromatic light at 700 nm with an intensity of 4.5 mW cm^{-2} was used for the continuous irradiation, if necessary.

We applied DSPC-AIGSSe@GaS_x liposomes with Se/(S+Se) = 0.5 to *in vivo* imaging. The details of the experimental procedures were the same as those reported previously.[23] The dispersions of DSPC-AIGSSe@GaS_x liposomes were diluted with phosphate-buffered saline (PBS) (pH 7.4) to give QD concentrations of 8.0, 4.0, 2.0, and 1.0 μmol(QDs) dm^{-3}. Mice (C57BL/6), purchased from Japan SLC (Hamamatsu, Japan), were housed in a controlled environment (12-h light/dark cycles at 22 °C) with *ad libitum* access to water and a standard chow diet before they were sacrificed. The conditions and the handling of the animals in this study were approved by the Nagoya University Committee on Animal Use and Care. A 50-mm^3 portion of each DSPC-AIGSSe@GaS_x liposome dispersion was injected subcutaneously in the back of a mouse under anesthesia. PL signals were detected with an *in vivo* PL imaging system (IVIS Spectrum CT; excitation filter, 720 nm; emission filter, 790 nm long-pass). For acquiring *in vivo* real-time PL images, a fluorescent video imaging system (IVIS Lumina K Series III for video images) was used with an excitation filter of 720 nm and an emission filter of 790 nm long-pass.

Cytotoxicity Testing of DSPC-AIGSSe@GaS_x

The cytotoxicity of DSPC-AIGSSe@GaS_x liposomes was investigated with previously reported methods.[23,51] Human squamous carcinoma A431 cells (2×10^4 cells) were seeded in 96-well plates (BD Biosciences) with 0.10 cm^3 of culture medium at 37 °C. After the incubation for 24 h, the cells were transduced with DSPC-AIGSSe@GaS_x liposomes of Se/(S+Se)= 0 and 0.50 in transduction medium (0.10 cm^3) for 24 h. The medium was changed to new transduction medium (0.10 cm^3), and the Cell Counting Kit-8 (CCK-8; DOJINDO Laboratories, Japan) was used for counting viable cells. The CCK-8 regent (0.01 cm^3) was put into each well. After the reaction was allowed to proceed for 2 h, the absorbance of the sample was measured at 450 nm against a background control using a microplate reader.

Results and Discussion

Composition-dependent optical properties of AIGSSe and AIGSSe@GaS_x QDs

The two-step heating process in the synthesis was important to obtain highly photoluminescent AIGSSe QDs. TEM images of the particles obtained after the first heat treatment at 100 °C and those obtained with further heating at 250 °C for 30 min are shown in Fig. 1. As shown in Fig. 1a, the particles heat-treated at 250 °C for 30 min were spherical or polygonal particles and

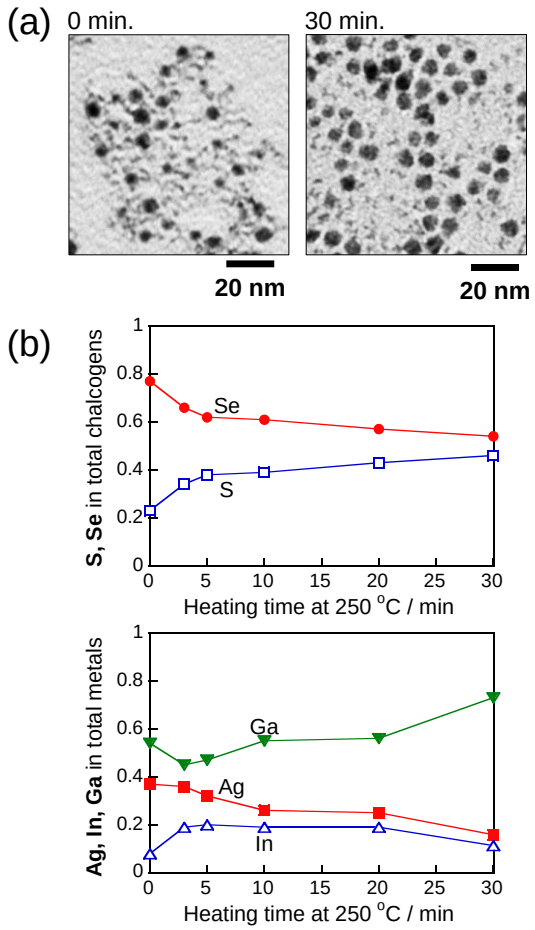

Fig. 1. (a) TEM images of particles with the second heat treatment at 250 °C for 0 and 30 min. (b) Changes in the chemical composition of particles obtained with different second heating times. The reaction time just after the first heat treatment at 100 °C is represented as 0 min in the panels.

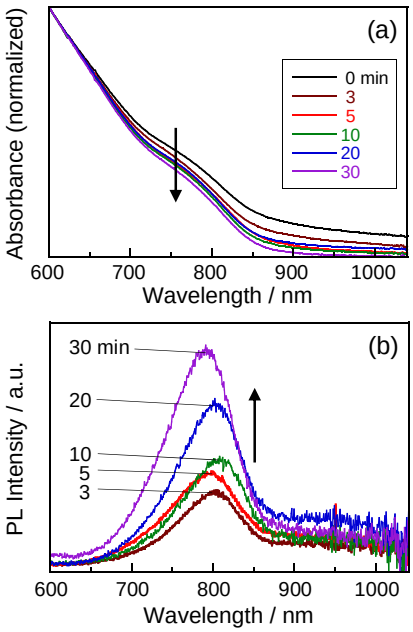

Fig. 2. Absorption spectra (a) and PL spectra (b) of AIGSSe QDs with different reaction times in the second heat treatment at 250 °C.

had a relatively narrow size distribution with an average diameter (d_{av}) of 3.8 nm and standard deviation (σ) of 1.0 nm. In contrast, the particles formed after the first heat treatment were a mixture of spherical particles of 2.7 ± 0.58 nm in size and thin bent wire-like particles. XRD measurements (Fig. S1) revealed that the particles formed after the first heat treatment exhibited XRD patterns assignable to a mixture of cubic Ag_2Se phase and monoclinic Ag_2S phase and that such particles disappeared during the second heat treatment at 250 °C for 30 min, resulting in the formation of QDs having a tetragonal crystal structure, the diffraction peaks of which were shifted to a higher angle than those corresponding to $AgInSe_2$ due to the content of S^{2-} and Ga^{3+}. These observations suggested that a large number of Ag_2Se and Ag_2S nanocrystals formed with the first heat treatment and then acted as nuclei to dope S, In and Ga in the second heat treatment at 250 °C, resulting in the production of Ag-(In,Ga)-(S,Se) (AIGSSe) QDs. It should be noted that the QDs prepared in the absence of a Ga precursor had a larger size and exhibited little photoluminescence (not shown), suggesting that the addition of a Ga precursor, preventing rapid crystal growth, was necessary to prepare mixed-anion I-III-VI QDs with high quality.

The change in composition was confirmed by elemental analysis of particles. Figure 1b shows the change in the chemical composition of QDs obtained with different heating times at 250 °C. The QDs obtained after the first heating at 100 °C contained a large fraction of Se in total chalcogenides, 0.77, while the fraction of Ag in total metals was 0.37, which agreed with that used for preparation, 0.40. With the elapse of heating time at 250 °C, the fraction of Se in QDs was decreased by the increase of S doping, and the fraction of Se finally reached 0.54, being in agreement with that of precursors used for preparation, 0.50. On the other hand, the fraction of Ag in total metals decreased from 0.37 to 0.16 with an increase in the heating time from 0 to 30 min, the latter value of which was much smaller than the Ag fraction in the metal precursors, 0.40. In contrast, the In fraction was initially increased from 0.08 to 0.20 with the elapse of heating time from 0 to 10 min and decreased to 0.11 with prolonged heat treatment up to 30 min. The Ga fraction tended to increase to 0.73 from the initial value of 0.55 with the elapse of heating time, while it was slightly decreased with heat treatment for the initial 3 min.

The optical properties of QDs were significantly varied depending on the time for heating at 250 °C. Figure 2 shows the absorption spectra and PL spectra of QDs with various heating times at 250 °C. The QDs obtained with only the first heat treatment at 100 °C exhibited a broad absorption spectrum, the onset wavelength of which was longer than 1000 nm, and then showed no photoluminescence. This suggested that nanocrystals of a smaller energy gap (E_g), such as silver chalcogenides, were formed and acted as non-radiative recombination sites. With an increase in the time of the second heat treatment at 250 °C, the absorbance at a wavelength longer than 850 nm drastically decreased, accompanied by a

blue shift of the onset wavelength to ca. 860 nm. An absorption shoulder assignable to the exciton peak appeared at 780 nm. It should be noted that a small amount of absorption tail still remained in the wavelength region longer than 850 nm, even after heating for 30 min. This probably corresponded to the presence of a small amount of bent wire-like particles in the sample as shown in the TEM image (Fig. 1a, right panel). Furthermore, heating at 250 °C caused the emergence of a PL peak originating from the band-edge emission at 790 nm, the intensity being enlarged with the elapse of heating time probably due to the decrease of crystal defects. Thus, we concluded that the reaction time, 30 min, used in the second heat treatment at 250 °C was long enough to synthesize AIGSSe QDs with high crystallinity.

The optical properties of AIGSSe QDs were controlled in the visible and near-IR wavelength regions by changing the chalcogen composition. With an increase in the Se/(S+Se) ratio in the precursors, the Se fraction of obtained QDs linearly increased (Fig. S2 and Table S1). It should be noted that the composition of chalcogens included S atoms derived from DDT ligands adsorbed on the QD surface. In the case of the Se/(S+Se)= 1.0, the AIGSSe QDs were prepared without the addition of S in the chalcogen precursor, but the elemental analysis revealed that resulting QDs contained the small amount of S atoms, 2%, originating from DDT ligands (Table S1). In contrast, although the ratio of Ag:In:Ga in the preparation was fixed to 0.40:0.24:0.36, the AIGSSe QDs prepared with Se/(S+Se)= 0.50 or smaller had an almost constant ratio of Ag:In:Ga= 0.17:0.11:0.72, being a remarkable Ga-rich composition. The QDs prepared with Se/(S+Se)= 1.0 contained a slightly smaller Ga fraction of 0.58 than those of QDs prepared with other Se/(S+Se) ratios. Figure 3a shows the absorption spectra of AIGSSe QDs. The absorption onset was blue-shifted from 856 nm to 651 nm with a decrease in the Se/(S+Se) ratio in the preparation from 0.50 to 0, while the QDs prepared with Se/(S+Se)=1.0, that is, Ag-In-Ga-Se QDs, exhibited an onset wavelength at 828 nm, being slightly shorter than that of AIGSSe QDs with Se/(S+Se)=0.50. The absorption spectra were structureless for the QDs prepared with Se/(S+Se) = 0.14 or less, but the AIGSSe QDs prepared with Se/(S+Se) = 0.50 and 1.0 exhibited shoulders at 780 and 750 nm, respectively, being assignable to the exciton absorption peak. Figure 3e shows the E_g of QDs as a function of the Se/(S+Se) ratio in the preparation, determined from the absorption onset wavelength. With an increase in the Se/(S+Se) ratio from 0 to 0.50, the E_g of AIGSSe QDs monotonously decreased from 1.90 to 1.45 eV, while the E_g was inversely enlarged from 1.45 to 1.50 eV by increasing the Se/(S+Se) ratio from 0.50 to 1.0. This phenomenon is due to the band gap bowing effect originating from alloy formation, in which the E_g of the alloy was sometimes smaller than those of counterparts before alloying, because of the nonlinear relationship between E_g and the chemical composition of the alloy.

Figure 3b shows the PL spectra of AIGSSe QDs. Regardless of the Se/(S+Se) ratio, AIGSSe QDs exhibited a relatively sharp band-edge PL peak near the onset wavelength of the corresponding absorption spectrum, accompanied by a broad

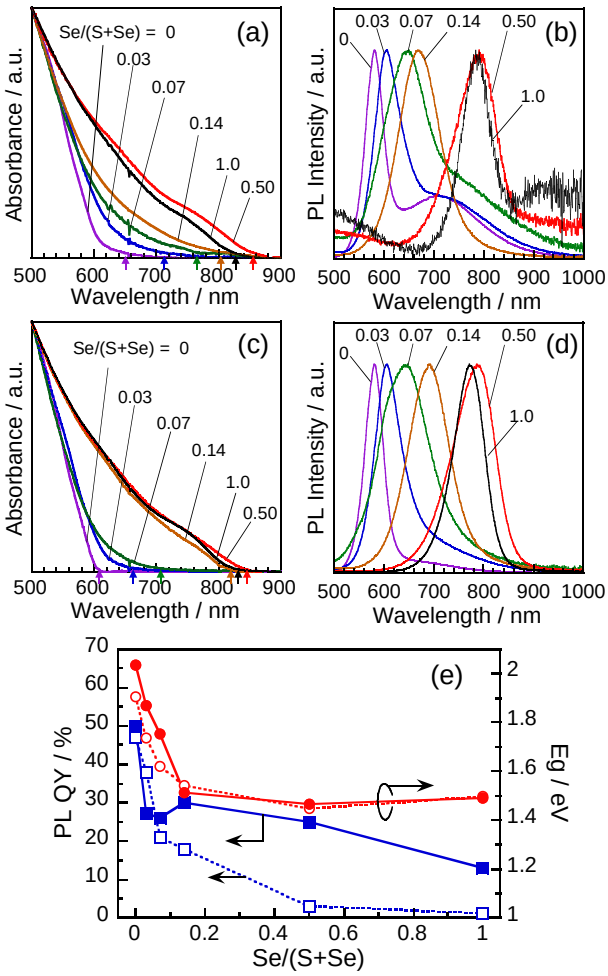

Fig. 3. Absorption spectra (a,c) and PL spectra (b,d) of QDs prepared with different Se/(S+Se) ratios. Samples were AIGSSe QDs (a,b) and AIGSSe@GaS_x QDs (c,d). Arrows in panels a and c represent the onset wavelengths of individual spectra. (e) Dependences of Eg (circles) and PL QY (squares) of AIGSSe QDs (open symbols) and AIGSSe@GaS_x QDs (solid symbols) on the Se/(S+Se) ratio in the preparation.

PL peak originating from defect sites on the longer wavelength side of the band-edge peak except for the case with Se/(S+Se)= 0.14. The peak position of the band-edge PL was dependent on the Se/(S+Se) ratio and was blue-shifted from 790 to 580 nm with an increase in the E_g of QDs, being similar to the behavior of their absorption onset. We previously reported that the defect-site emission of multinary QDs, such as $AgInS_2$,[52] $Ag(In,Ga)S_2$[42] and $Ag(In,Ga)Se_2$[42] was successfully eliminated by surface coating with GaS_x of higher E_g, in which the resulting core-shell QDs showed a sharp band-edge emission with a higher PL quantum yield (QY). Thus, we applied a similar strategy to AIGSSe QDs for improving their PL properties.

The process of GaS_x surface coating on AIGSSe QDs unexpectedly modified their absorption spectra, being different from the cases of $Ag(In,Ga)S_2$[42] and $Ag(In,Ga)Se_2$[42] QDs reported in our previous papers, as shown in Fig. 3c. The absorption onsets of AIGSSe@GaS_x QDs with Se/(S+Se) of 0.07 or less were blue-shifted by the GaS_x coating, indicating an increase in E_g of AIGSSe QDs by GaS_x coating (Fig. 3e) probably due to the slight doping of Ga and/or S into the cores. In contrast, the absorption

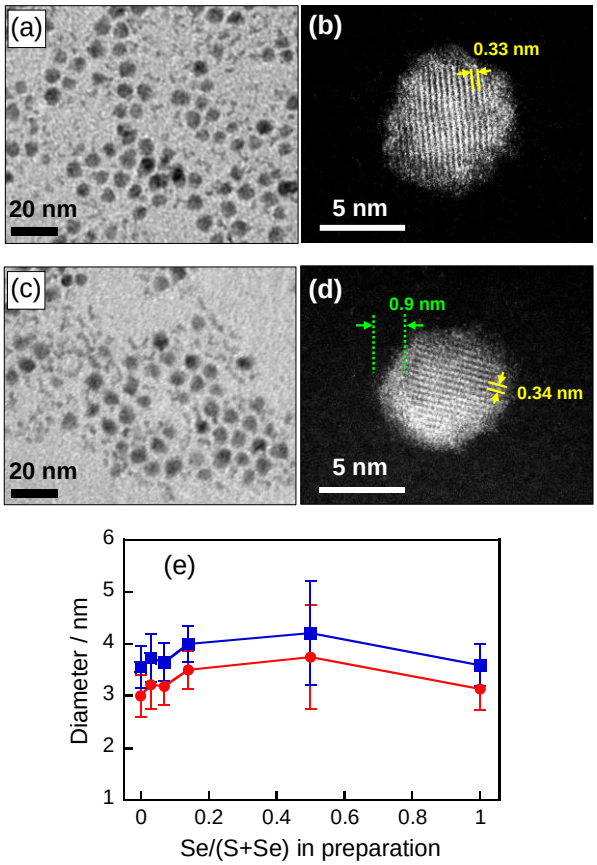

Fig. 4. Wide-area TEM (a,c) and HAADF-STEM images (b,d) of QDs. Samples were AIGSSe QDs prepared with Se/(S+Se)= 0.50 (a,b) and those surface-coated with a GaS_x shell (c,d). (e) Dependence of the average sizes of AIGSSe QDs (circles) and AIGSSe@GaS_x (squares) on the Se/(S+Se) ratio in the preparation.

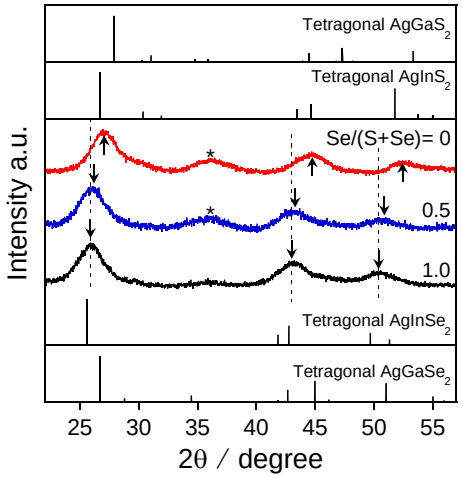

Fig. 5. XRD patterns of AIGSSe QDs prepared with different Se/(S+Se) ratios. The peaks marked as asterisks were assigned to the Ga_2O_3 crystal phase contained as a by-product.

spectrum of AIGSSe@GaS_x QDs with Se/(S+Se)=0.14 became more structured than that before GaS_x coating, suggesting that the crystallinity of cores was improved by the higher heat treatment at 300 °C during the surface coating. The QDs prepared with Se/(S+Se)=0.50 and 1.0 exhibited almost unchanged absorption spectra before and after surface coating. Figure 3d shows the PL spectra of AIGSSe@GaS_x QDs. The band-edge emission peaks became prominent with GaS_x coating, while the intensity of a broad defect-site PL peak was remarkably diminished, regardless of the Se/(S+Se) ratio used for the preparation. The PL QYs, calculated from the sum of band-edge and defect-site emissions, are also plotted in Fig. 3e. The PL QYs were significantly enlarged by GaS_x coating, and the optimal value, 50%, was obtained for the band-edge emission of AIGSSe@GaS_x with Se/(S+Se) = 0. These results indicated that the surface sites showing a broad defect-site emission and/or acting as carrier recombination sites were successfully removed by the formation of GaS_x shell layers on AIGSSe cores.

The morphology of AIGSSe QDs was investigated by TEM measurements. As shown in Figs. 4a and S3, AIGSSe QDs were spherical particles with a narrow size distribution, regardless of the Se/(S+Se) ratio in the preparation. The average size of QDs varied slightly from 3.0 to 3.8 nm as shown in Fig. 4e depending on the Se/(S+Se) ratio. The surface coating of these QDs with GaS_x slightly increased the average size to 3.5~4.2 nm (Fig. 4c and e). The thickness of the GaS_x layer was estimated to be 0.23~0.28 nm from half of the difference between the average diameters of AIGSSe QDs and AIGSSe@GaS_x QDs. We confirmed the presence of a shell layer by obtaining HAADF-STEM images of QDs. As shown in Fig. 4b, clear lattice fringes were observed in AIGSSe QD prepared with Se/(S+Se)= 0.50, the lattice spacing of which was 0.33 nm assignable to the interplanar spacing of (112) planes of the tetragonal crystal structure of $Ag(In,Ga)(S,Se)_2$, 0.34 nm, determined from XRD measurement as mentioned below. However, lattice fringes were not observed within ca. 0.5 nm below the surface, suggesting the presence of an amorphous surface layer without post-synthetic coating with a GaS_x shell layer. On the other hand, a shell layer was more clearly observed in the HAADF-STEM image of an AIGSSe@GaS_x QD (Fig. 4d): the AIGSSe nanocrystal, showing lattice fringes with spacing of 0.34 nm, was covered by an amorphous layer of ca. 0.9 nm in thickness. It should be noted in Fig. 4b and d that the thickness of the surface amorphous layer of the AIGSSe@GaS_x QD was larger by ca. 0.4 nm than that observed for the AIGSSe QD used as a core but that the increment of the amorphous layer with a GaS_x coating roughly agreed with the shell thickness estimated from the size difference of QDs before and after the GaS_x treatment (Fig. 4e). We simultaneously carried out nanoscale EDS analysis during the HAADF-STEM measurement. The central part of AIGSSe@GaS_x QDs had the composition of Ag/In/Ga/S/Se=30/20/6.4/8.9/34, giving the ratios of Ga/metals=0.11 and S/chalcogens=0.21. The chemical composition near the surface of AIGSSe@GaS_x QDs was Ag/In/Ga/S/Se=28/14/13/19/26, in which the ratios of Ga/metals and S/chalcogens were calculated to be 0.23 and 0.42, respectively, being larger than those corresponding to the central part of QDs. These results suggested that GaS_x was deposited as a shell layer on the AIGSSe QD core, being similar

to the cases of $Ag(In,Ga)S_2@GaS_x$[42] and $Ag(In,Ga)Se_2@GaS_x$[23] QDs in our previous studies. It should be noted that individual AIGSSe cores had smaller fractions of Ga and S than those obtained from the ensemble measurement of QDs, that is, the Ga and S fractions in the core of AIGSSe@GaS_x QDs, Ga/metals= 0.11 and S/chalcogens=0.21 determined by nanoscale EDS analysis, were much smaller than those obtained with AIGSSe (Se/(S+Se)=0.50) QD powders, Ga/metals= 0.62 and S/chalcogens=0.46, respectively, in Fig. 1b. These results suggested the AIGSSe QDs had a gradient-alloyed structure and were not composed of a homogeneous alloy: The doping rates of Ga and S atoms into nanocrystal cores were relatively slow and these elements were unevenly distributed in the AIGSSe QDs, resulting in the formation of an amorphous surface layer as shown in Fig. 4b.

Figure 5 shows XRD patterns of AIGSSe QDs. The observed diffraction peaks were broad for each of them because of their small particle size. The QDs prepared with only selenourea, Se/(S+Se)= 1.0, exhibited a diffraction pattern assignable to a tetragonal structure, in which each diffraction peak was located between those corresponding to tetragonal $AgInSe_2$ and $AgGaSe_2$ crystal structures. Furthermore, diffraction peaks of QDs prepared with only thiourea, Se/(S+Se)=0, appeared between those corresponding to tetragonal $AgInS_2$ and $AgGaS_2$ crystal structures. The individual peaks of QDs with Se/(S+Se)= 0 were located at higher diffraction angles than those with Se/(S+Se)= 1.0, indicating a decrease in the lattice constant of the tetragonal crystal structure due to the replacement of Se^{2-} with S^{2-} of a smaller ionic radius. These results indicated that solid solutions of $Ag(In,Ga)Se_2$ or $Ag(In,Ga)S_2$ were successfully prepared with the present synthetic conditions when single component chalcogen precursors, that is, selenourea or thiourea, were used for the preparation. In contrast, mixed-anion AIGSSe QDs prepared with Se/(S+Se)= 0.50 also exhibited diffraction peaks assignable to a tetragonal crystal structure, in which each peak was located between those corresponding to QDs with Se/(S+Se)= 0 and 1.0, but the peak shift from the corresponding peak of the $Ag(In,Ga)Se_2$ counterpart was small. These results also supported the gradient alloying for AIGSSe QDs with Se/(S+Se)= 0.50: The S^{2-} ions were inhomogeneously incorporated in the AIGSSe QDs and then the lattice spacings of most of the nanocrystal cores were larger than those expected from a homogeneously alloyed AIGSSe nanocrystal with Se/(S+Se)= 0.50. It should be noted that the XRD patterns with Se/(S+Se)= 0 and 0.50 also show a diffraction peak at around 36° assignable to a Ga_2O_3 crystal structure, suggesting that the powers of thus-obtained QDs contained Ga_2O_3 nanoparticles as a by-product, which also increased the fraction of Ga in the chemical composition obtained with the ensemble measurement of QDs.

Alloy formation of quinary AIGSSe was also confirmed by measuring the change in the electronic energy structure of QDs. We determined the ionization energy of obtained AIGSSe QDs from the onset energy of the PYSA spectra (Fig. S4). In the case of a semiconductor, the energy level of the valence band maximum (VBM) is assumed to be equal to be the opposite sign of the ionization energy, and the conduction band minimum

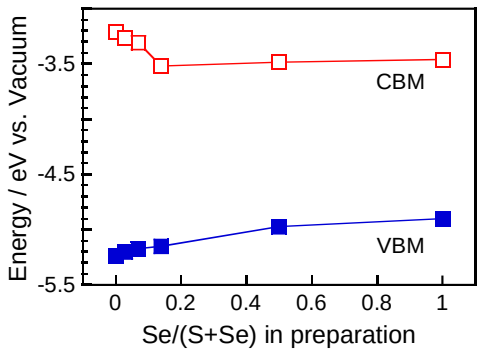

Fig. 6. Energy levels of the conduction band minimum (CBM) and the valence band maximum (VBM) of AIGSSe QDs as a function of the Se/(S+Se) ratio in the preparation.

(CBM) level is obtained by subtracting the corresponding E_g value from the VBM. Thus-obtained levels of VBM and CBM are plotted in Fig. 6 as a function of the Se/(S+Se) ratio in the preparation. It was clearly found that the VBM level was gradually shifted to a lower energy with a decrease in the Se/(S+Se) ratio, while the CBM level was almost constant at ca. -3.5 eV with Se/(S+Se)= 0.14 or larger but was shifted to a higher energy with a decrease in the Se/(S+Se) ratio from 0.14. The controllability of energy levels for present mixed-anion AIGSSe QDs was different from that previously reported for mixed-cation $Ag(In,Ga)Se_2$,[23] that is, the VBM level of AIGSSe QDs was tunable with the anion ratio, Se/S, without changing the metal composition, whereas the VBM was constant but the CBM was modified with the Ga/In ratio in $Ag(In,Ga)Se_2$ QDs. It was reported that the VBM was composed of hybrid orbitals between Ag 4d and S 3p orbitals for $AgInS_2$[53-55] and between Ag 4d and Se 4p orbitals for $AgInSe_2$,[56, 57] in which the energy level of the S 3p orbital was lower than that of the Se 4p orbital. Furthermore, Maeda and co-workers reported the electronic energy structures of bulk $Cu(In,Ga)(S,Se)_2$ powders, in which the levels of VBM and CBM were shifted to lower and higher energies, respectively, with an increase in the S fraction in particles even under the condition of a constant Ga/In ratio, because the S 3p orbital contributed to hybrid orbitals forming both VBM and CBM levels and then replacing S with Se modified the energies of both levels.[58] Considering the similarity between $Cu(In,Ga)(S,Se)_2$ and $Ag(In,Ga)(S,Se)_2$, the change in the electronic energy structure of AIGSSe QDs in Fig. 6 was reasonable even though the In fraction of AIGSSe QDs with Se/(S+Se)=1.0 was slightly larger than those of other QDs (Fig. S2). Thus, it was concluded that control of the S/Se ratio in mixed-anion AIGSSe QDs enabled modification of both levels of VBM and CBM as well as photoluminescence properties without significantly changing their metal composition ratio or particle size.

PL stability of AIGSSe@GaS$_x$ dispersed in aqueous solutions and its application for *in vivo* imaging

The stability of PL is an important factor for application to bioimaging. The present QDs were surface-modified with a dodecanethiol layer showing hydrophobicity and could not be uniformly dispersed in aqueous solutions. It has been reported that DSPC liposomes acted as a carrier to transfer hydrophobic QDs into an aqueous solution without significant aggregation.[23, 59] In the present study, we prepared DSPC liposomes containing AIGSSe@GaS$_x$ QDs (DSPC-AIGSSe@GaS$_x$) with a reported strategy. The average liposome size of synthesized DSPC-AIGSSe@GaS$_x$, determined by dynamic light scattering (DLS) measurement, was 137 nm, which was smaller than those previously prepared with AIGSe@GaS$_x$ and AgInTe$_2$, 179 and 180 nm, respectively, in our studies.[23, 59] A typical TEM image of DSPC-AIGSSe@GaS$_x$ (Se/(S+Se)= 0.50) is shown in Fig. S5a. Since the TEM samples were dried before measurement, the QDs in a liposome were observed as a large aggregate of ca. 110 ~ 150 nm in diameter, being comparable with that obtained with the DLS measurement. The onset wavelength of absorption spectrum of AIGSSe@GaS$_x$ QDs was almost unchanged after the incorporation into liposomes (Fig. S5b), suggesting that the size of individual QDs was not varied.

Figure 7 shows the PL spectra of DSPC-AIGSSe@GaS$_x$ liposome dispersions prepared with Se/(S+Se)= 0 and 0.50. Although the AIGSSe@GaS$_x$ used exhibited a narrow band-edge PL peak in chloroform regardless of the Se/(S+Se) ratio, the DSPC-AIGSSe@GaS$_x$ dispersions prepared with Se/(S+Se)= 0 showed a broad PL peak around 700 nm assignable to a defect-site emission as well as the band-edge emission at 580 nm. The relative intensity of the broad PL peak was larger in air than in an N_2 atmosphere. In contrast, mixed-anion QD-incorporated liposomes, that is, DSPC-AIGSSe@GaS$_x$ with Se/(S+Se)= 0.50, exhibited only a band-edge PL peak at 795 nm in both conditions, though a slight red shift of the PL peak by ca. 5 nm was observed from that of AIGSSe@GaS$_x$ QDs in chloroform, 790 nm. The chemical composition near the surface of AIGSSe@GaS$_x$ QDs, Ag/In/Ga/S/Se= 28/14/13/19/26, determined by nanoscale EDS analysis as mentioned above, suggested that a certain amount of Se was contained in the shell layer. Thus, the improvement of PL stability of QDs probably originated from preventing the dissolution of the GaS$_x$ shell layer in an aqueous solution via Se doping. The DSPC-AIGSSe@GaS$_x$ liposomes prepared with Se/(S+Se)= 0.50 exhibited a narrow band-edge PL peak in the first biological near-IR window. Their PL QY was as high as 19%, which was slightly decreased from that for AIGSSe@GaS$_x$ QDs in chloroform, 25%, probably due to the formation of aggregated particles in liposomes as shown in Fig. S5a, but considerably higher than that previously reported by us for Ag-(In,Ga)-Se@GaS$_x$ QDs incorporated in liposomes, 6.2%.[23]

We investigated the PL stability of aqueous dispersions of DSPC-AIGSSe@GaS$_x$ liposomes prepared with Se/(S+Se)= 0.50 under various conditions. Figure 8a shows the change in PL spectra of DSPC-AIGSSe@GaS$_x$ dispersions stored in the dark under an air atmosphere. The PL intensity gradually decreased

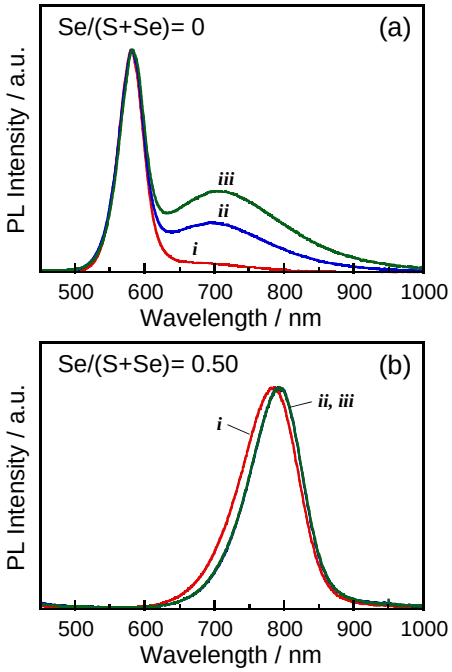

Fig. 7. PL spectra of AIGSSe@GaS$_x$ QDs uniformly dissolved in chloroform and DSPC-AIGSSe@GaS$_x$ liposomes dispersed in aqueous solutions. The AIGSSe cores used were prepared with Se/(S+Se)= 0 (a) and 0.50 (b). The samples were AIGSSe@GaS$_x$ QDs in chloroform (i) and freshly prepared DSPC-AIGSSe@GaS$_x$ aqueous dispersions under an N_2 atmosphere (ii) and in air (iii).

over time, but the peak shape of the band-edge emission was almost unchanged and no additional PL peaks originating from defect-site emission emerged. These results indicated that defect sites were formed in the shell layer or on the core surface during storage and then acted as non-radiative recombination sites but not as radiative ones. Similar behavior was observed for the QD liposomes of Se/(S+Se)= 0 with storage in air, as shown in Fig. S6. Although the PL intensity of QDs was almost unchanged under an N_2 atmosphere, only the band-edge PL peak of QDs significantly decreased during storage in air for 14 days. These suggested that the prolonged exposure of AIGSSe@GaS$_x$ (Se/(S+Se)= 0) QDs to O_2 in air increased the amount of defect sites, resulting in the enlargement of the relative intensity of broad PL peak as shown in Fig. 7a.

To confirm the potential ability of AIGSSe@GaS$_x$ in biological imaging, DSPC-AIGSSe@GaS$_x$ liposome dispersions were injected into the back of a mouse. As shown in Fig. 8b, PL emission was detected from the QDs through the skin, and the PL intensity was proportional to the concentration of QDs injected (Fig. S7). Despite the fact that the PL intensity rapidly decreased, we were still able to detect the PL signal of QDs from the mouse at 24 h after the injection. The PL intensity of QDs at 24 h after the injection was also proportional to concentration of QDs injected, but the detection sensitivity was remarkably reduced, because the slope of the linear relation decreased to 17% of the initial value. The DSPC-AIGSSe@GaS$_x$ liposomes exhibited PL intensity that was sufficient to obtain an *in vivo* three-dimensional PL image (S8 and Movie S1): the PL image

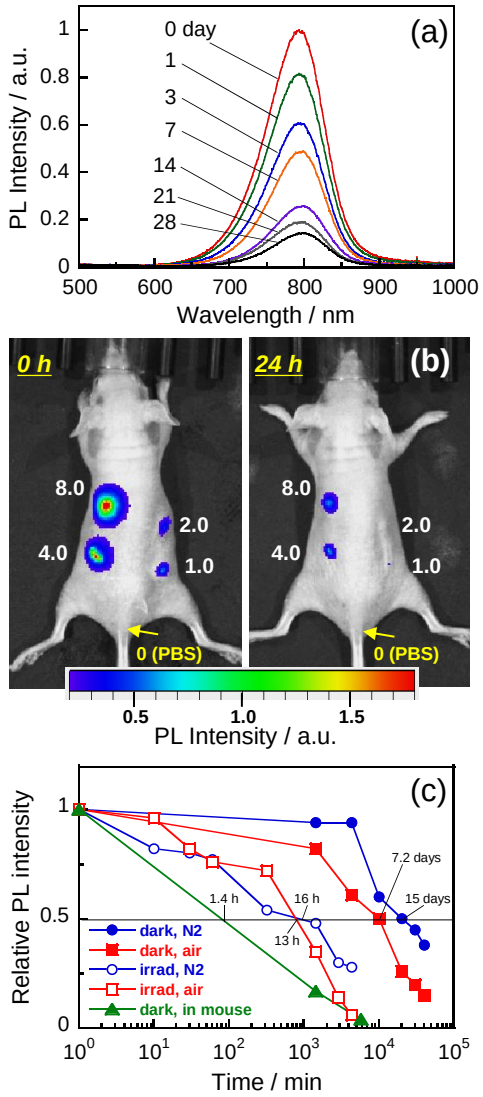

Fig. 8. (a) Changes in PL spectra of a DSPC-AIGSSe@GaS_x (Se/(S+Se)= 0.50) liposome aqueous dispersion stored in the dark under an air atmosphere. (b) *In vivo* PL images of the mouse subcutaneously injected with DSPC-AIGSSe@GaS_x dispersions (each 50 mm^3) in the back at 0 and 24 h. The numbers of the panels are the concentrations of QDs in the dispersions in the unit of μmol(QDs)/dm^3. (c) Time courses of band-edge PL intensity of DSPC-AIGSSe@GaS_x liposome dispersions under various conditions and of PL intensity of DSPC-AIGSSe@GaS_x liposomes injected into the back of the mouse. The measurements started at the 1st minute. Each PL intensity was normalized by the corresponding initial value. The dispersions were stored in air and under an N_2 atmosphere. Irradiation was carried out at room temperature, if necessary, with 700 nm monochromatic light, the intensity of which was 4.5 mW/cm^2.

was obtained from QDs located inside the body at several millimeters in depth and was superimposed on a simultaneously obtained X-ray CT image of the mouse. In addition, we easily obtained an *in vivo* real-time PL image of the mouse moving around by detecting the PL signal from DSPC-AIGSSe@GaS_x liposomes (Movie S2).

Figure 8c shows the changes in PL peak intensity of DSPC-AIGSSe@GaS_x (Se/(S+Se)= 0.50) liposome aqueous dispersions with the elapse of storage time. The dispersion stored under an N_2 atmosphere had PL intensity of more than 90% of the initial value even after storage for 3 days, although it rapidly decreased with further prolonged storage. The PL intensity of DSPC-AIGSSe@GaS_x liposomes in the dark under an air atmosphere decreased faster than that of liposomes stored under an N_2 atmosphere. Furthermore, continuous irradiation of monochromatic light at 700 nm with 4.5 mW/cm^2 more rapidly decreased the PL intensity of QDs in both air and an N_2 atmosphere, suggesting that non-radiative recombination sites were formed during the photooxidation of AIGSSe@GaS_x. The PL intensity of DSPC-AIGSSe@GaS_x liposomes (8 μmol(QDs) dm^{-3}) injected into the mouse is also plotted in Fig. 8c. PL signals were able to be detected from the mouse up to 4 days. The rate of decrease in the PL intensity was considerably faster in the mouse than in the aqueous dispersions: The half-life period of PL intensity in the mouse was estimated to be about 1.4 h by interpolation, being much shorter than the half-life periods in the dark under air and N_2 atmospheres, ca. 7.2 days and 15 days, respectively. These results indicated that the environmental condition inside living tissue was much more severe for AIGSSe@GaS_x QDs even though they were encapsulated in DSPC liposomes.

The toxicity of the QDs is an important factor for bioimaging application. We investigated the cytotoxicity of the present QDs with various concentrations on A431 cells. The cell viability decreased with an increase in the QD concentration (Fig. S9), the degree being slightly larger for the QDs with Se/(S+Se)= 0.50 than those with Se/(S+Se)= 0, but a >80% portion of the cells were still alive for both kinds of AIGSSe@GaS_x QDs after the exposure for 24 h. This indicated that the content of Se in QDs caused the decrease of the cell viability as previously reported,[60] but that the observed cytotoxicity was low enough to use DSPC-AIGSSe@GaS_x liposomes as a probe for bioimaging, compared with less-toxic QDs encapsulated in liposomes reported by recent studies.[61, 62]

Conclusions

We successfully developed a strategy for synthesis of mixed-anion I-III-VI-based AIGSSe QDs showing an intense band-edge PL peak. Even though the metal composition or particle size was not significantly changed, the absorption and photoluminescence properties were widely controllable in the visible and near-IR wavelength regions by modulating the S/Se ratio in QDs. The E_g increased from 1.5 to 1.9 eV with a decrease in the Se/(S+Se) ratio from 1.0 to 0, accompanied by shifts in the energy levels of VBM and CBM to lower energy and higher energy, respectively. The controllability of energy levels for mixed-anion AIGSSe QDs was based on the Se/S ratio and was different from that for mixed-cation Ag(In,Ga)Se_2 QDs, in which the VBM was almost constant but the CBM was shifted to higher level with an increase in the Ga/In ratio of Ag(In,Ga)Se_2.[23] Surface coating of AIGSSe QDs with GaS_x removed defect-site emission and then enhanced the band-edge intensity. AIGSSe@GaS_x QDs with Se/(S+Se) = 0.50 exhibited a sharp PL peak at 790 nm, being in a biological window that is suitable for *in vivo* imaging. To transfer QDs into aqueous solution, these

QDs were encapsulated with DSPC liposomes. The AIGSSe@GaS_x QDs with Se/(S+Se) = 0.50 maintained a sharp band-edge PL peak even in an aqueous dispersion, in which the PL QY was slightly decreased from 25% in chloroform to 19% in aqueous dispersions but was high enough to be used as a near-IR PL probe. In contrast, the incorporation of QDs with Se/(S+Se) = 0, that is, AIGS QDs, in liposomes resulted in the development of a broad PL peak in addition to the band-edge peak due to the formation of defect sites in the aqueous dispersion. We obtained three-dimensional *in vivo* PL images by injecting mixed-anion AIGSSe@GaS_x-incorporated liposomes under the skin of a mouse. Our findings will be important for designing I–III–VI semiconductor QDs with the formation of mixed-anion alloys and will contribute to wide ranging applications.

Conflicts of interest

There are no conflicts to declare.

Acknowledgements

This work was supported by JSPS KAKENHI Grant Numbers JP16H06507 in Scientific Research on Innovative Areas ''Nano-Material Optical-Manipulation'', and JP18H03927. T.K. thanks PRESTO, JST for the financial support (Grant Number JPMJPR18T5).

References

1. Kenry, Y. Duan and B. Liu, *Adv. Mater.*, 2018, **30**, 1802394.
2. G. Hong, A. L. Antaris and H. Dai, *Nat. Biomed. Eng.*, 2017, **1**, 0010.
3. R. G. Aswathy, Y. Yoshida, T. Maekawa and D. S. Kumar, *Anal. Bioanal. Chem.*, 2010, **397**, 1417-1435.
4. R. C. Somers, M. G. Bawendi and D. G. Nocera, *Chem. Soc. Rev.*, 2007, **36**, 579-591.
5. T. Aubert, S. J. Soenen, D. Wassmuth, M. Cirillo, R. Van Deun, K. Braeckmans and Z. Hens, *ACS Appl. Mater. Interfaces*, 2014, **6**, 11714-11723.
6. D. Saikia, S. Chakravarty, N. S. Sarma, S. Bhattacharjee, P. Datta and N. C. Adhikary, *Luminescence*, 2017, **32**, 401-408.
7. J. Wang, Y. Lu, F. Peng, Y. Zhong, Y. Zhou, X. Jiang, Y. Su and Y. He, *Biomaterials*, 2013, **34**, 9509-9518.
8. R. Hu, W.-C. Law, G. Lin, L. Ye, J. Liu, J. Liu, J. L. Reynolds and K.-T. Yong, *Theranostics*, 2012, **2**, 723-733.
9. D. Wang, J. Qian, F. Cai, S. He, S. Han and Y. Mu, *Nanotechnology*, 2012, **23**, 245701.
10. T. Jin, C. Huang, M. Cui, Y. Yang, Z. Wang, W. Zhu and X. Qian, *J. Mater. Chem. B*, 2020, **8**, 10686-10699.
11. H. Kobayashi, M. Ogawa, R. Alford, P. L. Choyke and Y. Urano, *Chem. Rev.*, 2010, **110**, 2620-2640.
12. A. P. Alivisatos, W. Gu and C. Larabell, *Annu. Rev. Biomed. Eng.*, 2005, **7**, 55-76.
13. U. Resch-Genger, M. Grabolle, S. Cavaliere-Jaricot, R. Nitschke and T. Nann, *Nat. Methods*, 2008, **5**, 763-775.
14. J. Sobhanan, P. Jones, R. Kohara, S. Sugino, M. Vacha, C. Subrahmanyam, Y. Takano, F. Lacy and V. Biju, *Nanoscale*, 2020, **12**, 22049-22058.
15. S. M. Kobosko, D. H. Jara and P. V. Kamat, *ACS Appl. Mater. Interfaces*, 2017, **9**, 33379-33388.
16. I. A. Mir, V. S. Radhakrishanan, K. Rawat, T. Prasad and H. B. Bohidar, *Sci. Rep.*, 2018, **8**, 9322.
17. E. Soheyli, B. Ghaemi, R. Sahraei, Z. Sabzevari, S. Kharrazi and A. Amani, *Mater. Sci. Eng. C-Mater. Biol. Appl.*, 2020, **111**, 110807.
18. Q. Xiong, J. Yang, H. Ding, J. Du, X. Tang, T. Shi, Z. Liu, D. Wu, H. Lin and Y. Leng, *J. Mater. Chem. C*, 2020, **8**, 8515-8520.
19. W. Yang, W. Guo, T. Zhang, W. Yang, L. Su, L. Fang, H. Wang, X. Gong and J. Chang, *J. Mater. Chem. B*, 2015, **3**, 8518-8527.
20. J.-Y. Chang, G.-Q. Wang, C.-Y. Cheng, W.-X. Lin and J.-C. Hsu, *J. Mater. Chem.*, 2012, **22**, 10609-10618.
21. A. Delices, D. Moodelly, C. Hurot, Y. Hou, W. L. Ling, C. Saint-Pierre, D. Gasparutto, G. Nogues, P. Reiss and K. Kheng, *ACS Appl. Mater. Interfaces*, 2020, **12**, 44026-44038.
22. M. Dai, S. Ogawa, T. Kameyama, K.-i. Okazaki, A. Kudo, S. Kuwabata, Y. Tsuboi and T. Torimoto, *J. Mater. Chem.*, 2012, **22**, 12851-12858.
23. T. Kameyama, H. Yamauchi, T. Yamamoto, T. Mizumaki, H. Yukawa, M. Yamamoto, S. Ikeda, T. Uematsu, Y. Baba, S. Kuwabata and T. Torimoto, *ACS Appl. Nano Mater.*, 2020, **3**, 3275-3287.
24. D. Deng, L. Qu and Y. Gu, *J. Mater. Chem. C*, 2014, **2**, 7077-7085.
25. M. A. Abate and J.-Y. Chang, *Sol. Energy Mater. Sol. Cells*, 2018, **182**, 37-44.
26. Q. Huang, K. Reuter, S. Amhed, L. Deligianni, L. T. Romankiw, S. Jaime, P. P. Grand and V. Charrier, *J. Electrochem. Soc.*, 2011, **158**, D57.
27. P.-H. Chuang, C. C. Lin and R.-S. Liu, *ACS Appl. Mater. Interfaces*, 2014, **6**, 15379-15387.
28. W. Yang, W. Guo, X. Gong, B. Zhang, S. Wang, N. Chen, W. Yang, Y. Tu, X. Fang and J. Chang, *ACS Appl. Mater. Interfaces*, 2015, **7**, 18759-18768.
29. T.-L. Li, Y.-L. Lee and H. Teng, *Energy Environ. Sci.*, 2012, **5**, 5315-5324.
30. D. Deng, Y. Chen, J. Cao, J. Tian, Z. Qian, S. Achilefu and Y. Gu, *Chem. Mater.*, 2012, **24**, 3029-3037.
31. W. Guo, N. Chen, C. Dong, Y. Tu, J. Chang and B. Zhang, *RSC Adv.*, 2013, **3**, 9470-9475.
32. C. Xia, W. Wu, T. Yu, X. Xie, C. van Oversteeg, H. C. Gerritsen and C. de Mello Donega, *ACS Nano*, 2018, **12**, 8350-8361.
33. S. Chang, Y. Zhao, J. Tang, Z. Bai, L. Zhao and H. Zhong, *J. Phys. Chem. C*, 2020, **124**, 6554-6561.
34. S. O. M. Hinterding, A. C. Berends, M. Kurttepeli, M.-E. Moret, J. D. Meeldijk, S. Bals, W. van der Stam and C. de Mello Donega, *ACS Nano*, 2019, **13**, 12880-12893.
35. W. Peng, J. Du, Z. Pan, N. Nakazawa, J. Sun, Z. Du, G. Shen, J. Yu, J.-S. Hu, Q. Shen and X. Zhong, *ACS Appl. Mater. Interfaces*, 2017, **9**, 5328-5336.
36. F. Khavari, J. Keller, J. K. Larsen, K. V. Sopiha, T. Törndahl and M. Edoff, *Phys. Status Solidi A-Appl. Res.*, 2020, **217**, 2000415.
37. J. Du, Z. Du, J.-S. Hu, Z. Pan, Q. Shen, J. Sun, D. Long, H. Dong, L. Sun, X. Zhong and L.-J. Wan, *J. Am. Chem. Soc.*, 2016, **138**, 4201-4209.
38. O. Yarema, M. Yarema, A. Moser, O. Enger and V. Wood, *Chem. Mater.*, 2020, **32**, 2078-2085.

39. G. Zaiats, S. Ikeda, S. Kinge and P. V. Kamat, *ACS Appl. Mater. Interfaces*, 2017, **9**, 30741-30745.
40. S. M. Kobosko and P. V. Kamat, *J. Phys. Chem. C*, 2018, **122**, 14336-14344.
41. J. Wang, T. Deng, D. Deng, R. Zhang, Y. Gu and X. Zha, *RSC Adv.*, 2016, **6**, 53760-53767.
42. T. Kameyama, M. Kishi, C. Miyamae, D. K. Sharma, S. Hirata, T. Yamamoto, T. Uematsu, M. Vacha, S. Kuwabata and T. Torimoto, *ACS Appl. Mater. Interfaces*, 2018, **10**, 42844-42855.
43. M.-Y. Chiang, S.-H. Chang, C.-Y. Chen, F.-W. Yuan and H.-Y. Tuan, *J. Phys. Chem. C*, 2011, **115**, 1592-1599.
44. T. Bai, C. Li, F. Li, L. Zhao, Z. Wang, H. Huang, C. Chen, Y. Han, Z. Shi and S. Feng, *Nanoscale*, 2014, **6**, 6782-6789.
45. H. J. Yun, J. Lim, A. S. Fuhr, N. S. Makarov, S. Keene, M. Law, J. M. Pietryga and V. I. Klimov, *ACS Nano*, 2018, **12**, 12587-12596.
46. H. Song, Y. Lin, M. Zhou, H. Rao, Z. Pan and X. Zhong, *Angew. Chem. Int. Ed.*, 2021, **60**, 6137-6144.
47. P.-Y. Hsieh, J.-Y. Wu, T.-F. M. Chang, C.-Y. Chen, M. Sone and Y.-J. Hsu, *Arab. J. Chem.*, 2020, **13**, 8372-8387.
48. Z. Lian, M. Sakamoto, H. Matsunaga, J. J. M. Vequizo, A. Yamakata, M. Haruta, H. Kurata, W. Ota, T. Sato and T. Teranishi, *Nat. Commun.*, 2018, **9**, 2314.
49. M. Sakamoto, T. Kawawaki, M. Kimura, T. Yoshinaga, J. J. M. Vequizo, H. Matsunaga, C. S. K. Ranasinghe, A. Yamakata, H. Matsuzaki, A. Furube and T. Teranishi, *Nat. Commun.*, 2019, **10**, 406.
50. O. Stroyuk, A. Raevskaya and N. Gaponik, *Chem. Soc. Rev.*, 2018, **47**, 5354-5422.
51. H. Yukawa, Y. Kagami, M. Watanabe, K. Oishi, Y. Miyamoto, Y. Okamoto, M. Tokeshi, N. Kaji, H. Noguchi, K. Ono, M. Sawada, Y. Baba, N. Hamajima and S. Hayashi, *Biomaterials*, 2010, **31**, 4094-4103.
52. T. Uematsu, K. Wajima, D. K. Sharma, S. Hirata, T. Yamamoto, T. Kameyama, M. Vacha, T. Torimoto and S. Kuwabata, *NPG Asia Mater.*, 2018, **10**, 713-726.
53. D. Huang and C. Persson, *Chem. Phys. Lett.*, 2014, **591**, 189-192.
54. K. Yamato, A. Iwase and A. Kudo, *ChemSusChem*, 2015, **8**, 2902-2906.
55. J. S. Jang, P. H. Borse, J. S. Lee, S. H. Choi and H. G. Kim, *J. Chem. Phys.*, 2008, **128**, 154717.
56. Y. Li, W. Fan, H. Sun, X. Cheng, P. Li and X. Zhao, *J. Appl. Phys.*, 2011, **109**, 113535.
57. D. Huang, C. Persson, Z. Ju, M. Dou, C. Yao and J. Guo, *Europhys. Lett.*, 2014, **105**, 37007.
58. T. Maeda, R. Nakanishi, M. Yanagita and T. Wada, *Jpn. J. Appl. Phys.*, 2020, **59**, SGGF12.
59. T. Kameyama, Y. Ishigami, H. Yukawa, T. Shimada, Y. Baba, T. Ishikawa, S. Kuwabata and T. Torimoto, *Nanoscale*, 2016, **8**, 5435-5440.
60. V. K. Sharma, T. J. McDonald, M. Sohn, G. A. K. Anquandah, M. Pettine and R. Zboril, *Chemosphere*, 2017, **188**, 403-413.
61. W. Lian, D. Tu, P. Hu, X. Song, Z. Gong, T. Chen, J. Song, Z. Chen and X. Chen, *Nano Today*, 2020, **35,** 100943.
62. K. Wiercigroch-Walkosz, J. Cichos, E. Wysokińska, G. Rotko, W. Kałas and M. Karbowiak, *Colloid Surf. A-Physicochem. Eng. Asp.*, 2019, **579**, 123631.